

Journal of Visualized Experiments

Exploring adipose tissue structure by methylsalicylate clearing and 3D imaging --Manuscript Draft--

Article Type:	Invited Methods Collection - JoVE Produced Video
Manuscript Number:	JoVE61640R1
Full Title:	Exploring adipose tissue structure by methylsalicylate clearing and 3D imaging
Keywords:	Adipose tissue; clearing; light microscopy; 3-D whole tissue; obesity; morphology
Corresponding Author:	Jérôme Gilleron FRANCE
Corresponding Author's Institution:	
Corresponding Author E-Mail:	gilleron@unice.fr
Order of Authors:	Jérôme Gilleron Cindy Meziat André Sulen Stoyan Ivanov Jennifer Jager David Estève Catherine Muller Jean-Francois Tanti Mireille Cormont
Additional Information:	
Question	Response
Please indicate whether this article will be Standard Access or Open Access.	Standard Access (US\$2,400)
Please indicate the city, state/province, and country where this article will be filmed . Please do not use abbreviations.	at the C3M in Nice, France

TITLE:

Exploring Adipose Tissue Structure by Methylsalicylate Clearing and 3D Imaging

AUTHORS & AFFILIATIONS:

Jérôme GILLERON¹, Cindy MEZIAT¹, André Sulen², Stoyan IVANOV³, Jennifer JAGER¹, David Estève⁴, Catherine Muller⁴, Jean-François TANTI¹ and Mireille CORMONT¹

¹Université Côte d'Azur, Inserm UMR1065, C3M, Team "Cellular and Molecular Pathophysiology of Obesity", Nice, France

²Integrated Cardio Metabolic Center, Department of Medicine, Karolinska Institutet, Stockholm, Sweden

³Université Côte d'Azur, Inserm UMR1065, C3M, Team "Haematometabolism in Diseases", Nice, France

⁴Institut de Pharmacologie et de Biologie Structurale (IPBS), Université de Toulouse, CNRS, UPS, Toulouse, France

gilleron@unice.fr

Cindy.MEZIAT@univ-cotedazur.fr

Andre.Sulen@uib.no

Stoyan.IVANOV@univ-cotedazur.fr

Jennifer.JAGER@univ-cotedazur.fr

David.Esteve@ipbs.fr

Catherine.Muller@ipbs.fr

Jean-Francois.TANTI@unice.fr

Mireille.Cormont@unice.fr

Correspondence to:

Jérôme Gilleron

jerome.gilleron@univ-cotedazur.fr

KEYWORDS:

Adipose tissue, clearing, light microscopy, 3-D whole tissue, obesity, morphology.

SUMMARY:

Here, we describe a simple, inexpensive and fast clearing method to resolve the 3D structure of both mouse and human white adipose tissue using a combination of markers to visualize vasculature, nuclei, immune cells, neurons, and lipid-droplet coat proteins by fluorescent imaging.

ABSTRACT:

Obesity is a major worldwide public health issue that increases the risk to develop cardiovascular diseases, type-2 diabetes, and liver diseases. Obesity is characterized by an increase in adipose tissue (AT) mass due to adipocyte hyperplasia and/or hypertrophy, leading to profound remodeling of its three-dimensional structure. Indeed, the maximal capacity of AT

to expand during obesity is pivotal to the development of obesity-associated pathologies. This AT expansion is an important homeostatic mechanism to enable adaptation to an excess of energy intake and to avoid deleterious lipid spillover to other metabolic organs, such as muscle and liver. Therefore, understanding the structural remodeling that leads to the failure of AT expansion is a fundamental question with high clinical applicability. In this article, we describe a simple and fast clearing method that is routinely used in the laboratory to explore the morphology of mouse and human white adipose tissue by fluorescent imaging. This optimized AT clearing method is easily performed in any standard laboratory equipped with a chemical hood, a temperature-controlled orbital shaker and a fluorescent microscope. Moreover, the chemical compounds used are readily available. Importantly, this method allows one to resolve the 3D AT structure by staining various markers to specifically visualize the adipocytes, the neuronal and vascular networks, and the innate and adaptive immune cells distribution.

INTRODUCTION:

Obesity is characterized by an increase in adipose tissue mass and has become a major worldwide public health issue, given that people with obesity have increased risk of developing cardiovascular disease, type-2 diabetes, liver diseases and some cancers.

A fundamental physiological function of adipose tissue is to modulate whole-body glucose and lipid homeostasis^{1,2}. During the feeding period, the adipocytes (i.e., the main cells of the adipose tissue) stores the excess glucose and lipids provided by a meal into triglycerides. During fasting, the adipocytes break down the triglycerides into non-esterified fatty acids and glycerol to sustain the energy demand of the body. During the development of obesity, adipose tissue expand by increasing the size (hypertrophia) and/or the number (hyperplasia) of adipocytes¹, to increase their storage capacity. When the expansion of adipose tissue reaches its limit, a constant highly variable among patients, the remaining lipids accumulates into other metabolic organs including muscles and liver^{3,4}, leading to their functional failure and initiating obesity-related cardio-metabolic complications^{1,5}. Therefore, identifying the mechanisms that govern adipose tissue expansion is a key clinical challenge.

The morphological modifications documented within adipose tissues during obesity are linked to its pathological dysfunction. Several staining procedures have been used to describe the tissue organization of the adipose tissue, including actin⁶, vascular markers⁷, lipid-droplet markers⁸, and specific immune cell markers^{9,10}. However, because of the huge diameter of adipocytes (50 to 200 μm)¹¹, it is essential to analyze a large portion of the whole tissue in three dimensions in order to accurately analyze the dramatic structural AT changes observed during obesity. However, because the light does not penetrate an opaque tissue, imaging in 3D within a large tissue samples using fluorescence microscopy is not possible. Methods of tissue clearing to make them transparent have been reported in the literature (for a review, see¹²) allowing one to clear tissues and to perform in-depth, whole tissue fluorescence microscopy. These methods offer unprecedented opportunities to assess the 3D cellular organization in healthy and diseased tissue. Each of the described methods have advantages and drawbacks, and therefore need to be carefully selected depending on the studied tissue (for a review, see¹³). Indeed, some approaches require a long incubation period and/or the use of materials or

compounds that are either expensive, toxic or difficult to obtain¹⁴⁻¹⁹. Taking advantage of one of the first compounds used a century ago by Werner Spalteholz to clear tissues²⁰, we set up a user-friendly and inexpensive protocol that is very well adapted for the clearing of all mouse and human adipose tissue depots in any laboratory with typical equipment including a chemical hood, a temperature-controlled orbital shaker and a confocal microscope.

PROTOCOL:

This protocol was tested and is validated for all mouse and human white adipose tissue depots. Human and mouse adipose tissues were collected accordingly to European laws and approved by French and Swedish Ethical committees.

1. Fixation of mouse and human white adipose tissue

1.1. Immerse the harvested mouse or human white adipose tissues in at least 10 mL of PBS containing 4% paraformaldehyde (PFA) in a 15 mL plastic tube.

1.2. Shake the plastic tube at room temperature on a rolling plate for 1 h.

1.3. Leave the plastic tube at 4 °C on a rolling plate overnight, to complete the fixation.

NOTE: This protocol is adapted for large adipose tissue samples, such as whole epididymal fat pads obtained from mice fed a normal diet (≈ 250 mg - ≈ 0.6 cm³). For larger samples like epididymal fat pads obtained from mice fed a high fat diet (≈ 1.5 g - ≈ 4 cm³) or human adipose tissue samples, although the clearing protocol should perfectly work for the whole sample (by scaling-up the PFA and the antibody mixtures), in general, we cut tissue pieces around 1 g (≈ 2.5 cm³) to reserve the remaining samples either for additional staining or applications. For the PFA (step 1.1.) we recommend using roughly 10 times the volume of the tissue. For the antibody mixtures (steps 3.1. and 3.4.), increase the volume to completely immerse the tissue, and use a 15 mL plastic tube (see **Table of Materials**) if the tissue is too large for a 1.5 mL plastic microtube (see **Table of Materials**).

2. Permeabilization and saturation of mouse and human white adipose tissue

2.1. Rinse the fixed white adipose tissue in 10 mL of PBS for 5 min at room temperature to remove all traces of PFA.

2.2. Immerse the tissue in a 15 mL plastic tube containing 10 mL of PBS supplemented with 0.3% glycine (see **Table of Materials**) and shake the tube at room temperature in an orbital shaker for 1 h at 100 revolutions per minute (rpm) to quench the remaining free aldehyde groups.

2.3. Immerse the tissue in a 15 mL plastic tube containing 10 mL of PBS supplemented with 0.2% Triton X-100 (see **Table of Materials**) and shake the tube at 37 °C in a temperature-

controlled orbital shaker for 2 h at 100 rpm.

2.4. Immerse the tissue in a 15 mL plastic tube containing 10 mL of PBS supplemented with 0.2% Triton X-100 and 20% DMSO (see **Table of Materials**) and shake the tube at 37 °C in a temperature-controlled orbital shaker at 100 rpm overnight.

2.5. Immerse the tissue in a 15 mL plastic tube containing 10 mL of PBS supplemented with 0.1% Tween-20 (see **Table of Materials**), 0.1% Triton X-100, 0.1% deoxycholate (see **Table of Materials**) and 20% DMSO and shake the tube at 37 °C in a temperature-controlled orbital shaker at 100 rpm for at least 24 h.

2.6. Rinse the tissue in a 15 mL plastic tube containing 10 mL of PBS supplemented with 0.2% Triton X-100 and shake the tube at room temperature in an orbital shaker at 100 rpm for 1 h.

2.7. Immerse the tissue in a 15 mL plastic tube containing 10 mL of PBS supplemented with 0.2% Triton X-100, 10% DMSO and 3% BSA (see **Table of Materials**) and shake the tube at 37 °C in a temperature-controlled orbital shaker at 100 rpm for 12 h, to saturate any sites that could non-specifically bind antibodies.

NOTE: In step 2.7, the BSA can be substituted by blood serum of the species of the secondary antibody used.

3. Staining procedure for mouse and human white adipose tissue

3.1. Transfer the tissue in a 1.5 mL plastic microtube containing 300 µL of PBS supplemented with 0.2% Triton X-100, 10% DMSO, 3% BSA and the primary antibodies (10x more concentrated than for cryosection staining but optimal antibody concentration should be evaluated for each antibody). Protect the tube from light by covering with aluminium foil and shake the tube at 37 °C in a temperature-controlled orbital shaker at 100 rpm for at least 2 days (see the note in step 1.1 and step 3.7.1).

3.2. Rinse the tissue in a 15 mL plastic tube containing 10 mL of PBS supplemented with 0.2% Triton X-100, 10% DMSO and 3% BSA and shake the tube protected from light at 37 °C in a temperature-controlled orbital shaker at 100 rpm for 5 h. Perform this step twice.

3.3. Rinse the tissue in a 15 mL plastic tube containing 10 mL of PBS supplemented with 0.2% Triton X-100, 10% DMSO and 3% BSA and shake the tube, protected from light, at 37 °C in a temperature-controlled orbital shaker at 100 rpm for one night to two days.

3.4. Transfer the tissue to a 1.5 mL plastic microtube containing 300 µL of PBS supplemented with 0.2% Triton X-100, 10% DMSO, 3% BSA and the secondary antibodies (10x more concentrated than for cryosection staining). Protect the tube from light by covering with aluminium foil and shake the tube at 37 °C in a temperature-controlled orbital shaker at 100 rpm for at least 2 days (see the note in step 1.1 and step 3.7.1).

3.5. Rinse the tissue in a 15 mL plastic tube containing 10 mL of PBS supplemented with 0.2% Triton X-100, 10% DMSO, and 3% BSA and shake the tube, protected from light, at 37 °C in a temperature-controlled orbital shaker at 100 rpm for 5 h. Perform this step twice.

3.6. Rinse the tissue in a 15 mL plastic tube containing 10 mL of PBS supplemented with 0.2% Triton X-100, 10% DMSO, and 3% BSA and shake the tube, protected from light, at 37 °C in a temperature-controlled orbital shaker at 100 rpm for one night to two days.

3.7. Rinse the tissue in a 15 mL plastic tube containing 10 mL of PBS and shake the tube, protected from light, at 37 °C in a temperature-controlled orbital shaker at 100 rpm for 2 h.

3.7.1. For the labelling of specific structures such as nuclei or actin, add 4',6-diamidino-2-phenylindole (DAPI or equivalent) and/or the fluorescently labelled-phalloidin at step 3.1. when only fluorescently labelled primary antibodies are used, or at step 3.4. when secondary antibodies are used.

NOTE: For the staining procedure, primary antibodies already conjugated with fluorochromes (like those used for flow cytometry) can be used and we recommend it for the gain of time and specificity. Indeed, even if mouse primary antibodies can be used followed by secondary anti-mouse antibodies, as we demonstrated it here, we have often observed non-specific staining of blood vessels due to circulating immunoglobulin. Therefore, to avoid this issue, primary antibodies that are already labelled are highly recommended and here we provide evidence that the antibodies used in flow cytometry are compatible with our procedure. However, in the specific case of an antigen that is expressed at low levels, a signal amplification step via secondary antibodies is mandatory; when the only available primary antibody is made in mouse, a cardiac-perfusion of the mice with PBS for at least 5 min at the sacrifice can remove a large proportion of circulating immunoglobulin and thus the non-specific staining.

4. Clearing procedure for mouse and human white adipose tissue

4.1. Immerse the tissue in a 15 mL plastic tube containing 10 mL of 50% ethanol and shake the tube, protected from light, at room temperature in an orbital shaker at 100 rpm for 2 h.

4.2. Immerse the tissue in a 15 mL plastic tube containing 10 mL of 70% ethanol and shake the tube, protected from light, at room temperature in an orbital shaker at 100 rpm for 2 h.

4.3. Immerse the tissue in a 15 mL plastic tube containing 10 mL of 95% ethanol and shake the tube, protected from light, at room temperature in an orbital shaker at 100 rpm for 2 h.

4.4. Immerse the tissue in a 15 mL plastic tube containing 10 mL of 100% ethanol and shake the tube, protected from light, at room temperature in an orbital shaker at 100 rpm for 2 h.

4.5. Immerse the tissue in a 15 mL plastic tube containing 10 mL of 100% ethanol and shake

the tube, protected from light, at room temperature in an orbital shaker at 100 rpm overnight.

4.6. Immerse the tissue in a 20 mL glass bottle with a plastic cap (see table of materials) containing 5 mL of methyl salicylate (see table of materials) under a chemical hood and shake the glass container, protected from light, at room temperature in an orbital shaker at 100 rpm for at least 2 h.

NOTE: The clearing procedure could be significantly accelerated (if necessary) by avoiding steps 4.3. and 4.5., although the final clearing quality would be slightly reduced.

5. 3D-confocal imaging of cleared white adipose tissue

5.1. Transfer the tissue to a metallic imaging chamber equipped with a glass bottom (see **Table of Materials**) under a chemical hood and fill the chamber with fresh methyl salicylate.

5.1.1. To secure the tissue in place, and thus to prevent it from floating or moving sideways in the chamber, apply multiple 18 mm round glass coverslips (see **Table of Materials**) on top of the tissue when mounting it into the chamber.

5.2. Place the imaging chamber on an inverted confocal microscope.

5.3. Image the tissue using a low magnification objective (e.g., 4x objective) to generate a few cm³ 3D maps of the whole adipose tissue or of the human tissue sample.

5.4. Select several areas for the tissue sampling at higher magnification. Typically, use a 20x long distance air objective that provides a good ratio between resolution and depth. We acquire large mosaic images with z-stacks between 600 and 2000 µm depth.

5.4.1. Use a long-distance objective to image deeper into the tissue.

6. Extraction of quantitative results from the 3D adipose tissue images

NOTE: The segmentation of the different structures and the subsequent extraction of the quantitative information from the 3D-image stack generated in point 5 can be performed using any of the many existing image analysis software options, either commercial or freeware. In the following points, we describe a strategy that is routinely used in our laboratory to extract quantitative information from 3D adipose tissue images using commercial software (see **Table of Materials**).

6.1. Convert the 3D stacks onto the software format to free-up memory space.

6.2. Segment the cells.

6.2.1. Open the **Cell** module of the software.

265
266 6.2.2. Change the **Cell Detection** setting to plasma membrane staining.
267

268 6.2.3. Choose the fluorescent channel of the marker used to delineate the cell periphery
269 (phalloidin which labels cortical actin or plasma membrane markers such as F4/80 for
270 macrophage, TCR- β for T cells, or cluster of differentiation CD proteins specific for immune cell
271 subtypes).
272

273 6.2.4. Set up the thresholds and provide a range of expected cell size (i.e., 1 to 200 μm for cell
274 detection).
275

276 6.2.5. Run the segmentation. A volume corresponding to the z-stack will be generated with the
277 segmented cells color-coded with a different color for each of the neighbouring cells.
278

279 6.2.6. Apply statistical filters (size, roundness, circularity, etc.) in the statistic tab to exclude
280 segmentation artefacts and/or to refine the segmented cells to the cell of interest based on
281 their size (i.e., 20-200 μm for adipocytes; 5-25 μm for macrophages; 1-3 μm for lymphocytes).
282

283 6.2.7. Extract measurements and quantitative data (volume, number, size, diameter, etc.) from
284 the statistics tab.
285

286 6.3. Segment cellular components (nuclei, vesicles, etc.) or vessels as a structure.
287

288 NOTE: Although the filament segmentation is very useful to study the connectivity of the
289 vessels, we use the surface module segmentation to extract data on the size, volume and
290 diameters of the vessels. Indeed, the quantification of the sizes of the vessels is lost when using
291 the filaments module.
292

293 6.3.1. Open the **Surface** module of the software.
294

295 6.3.2. Select the fluorescent channel of the marker used to specifically label the subcellular
296 component to reconstruct it in 3D.
297

298 6.3.3. Set up the thresholds and provide a range of the expected diameter size of the structure
299 (i.e., 0.5-5 μm for nuclei; 0-100 μm for vessels; etc.).
300

301 6.3.4. Run the segmentation. A volume with the segmented cellular structure will be
302 generated. Measurements and quantitative data (volume, number, size, diameter, etc.) can be
303 extracted from the statistics tab.
304

305 6.4. Segment the vessels as a tubular continuum.
306

307 NOTE: Although the filament segmentation is very useful to study the connectivity of the
308 vessels, we use the surface module segmentation to extract data on the size, volume and

diameters of the vessels. Indeed, the quantification of the sizes of the vessels is lost when using the filaments module.

6.4.1. Open the **Filaments** module of the software.

6.4.2. Select the fluorescent channel corresponding to the vessel staining.

6.4.3. Set up the thresholds for the fluorescence intensity and select the appropriate number of expected connecting nodes.

6.4.4. Run the segmentation. Filaments representing vessel network will be generated in 3D. Measurements can be extracted from the statistics tab, allowing to obtain quantitative data including vessel length, number of vessel branching, etc.

REPRESENTATIVE RESULTS:

Using the procedure described here and summarized in **Figure 1**, we were able to stain and optically clear human and mouse white adipose tissue as presented in **Figure 2A** and **Figure 2B**, respectively. The cleared tissue was transferred to the metallic imaging chamber to perform confocal imaging (**Figure 3A**). The clearing drastically improved the depth of the tissue images that we were able to acquire (**Figure 3B** and **Figure 3C**). The whole adipose tissue can be acquired in 3D at low magnification using a 4x objective (see **supplementary movie 1** and **supplementary movie 2**), to generate a 3D map, enabling to select the different areas to be acquired at high magnification using a 20x objective (**Figure 3D**). The high magnification images are acquired in 3D with a depth of 2 mm (**Figure 3E**).

This procedure enables the labelling of numerous general cell markers, including nuclei by using DAPI and actin by using fluorescently-labelled Phalloidin. Specific staining of lipid droplets and adipocytes can be achieved by using perilipin antibody (see table of materials; **Figure 4A**) and anti-Glut4 antibody (see table of materials; **Figure 4B**) respectively. Blood vessels can be detected by using either the CD31 antibody (see table of materials; **Figure 4C**) or by an intravenous injection of lectin-DyLight649 shortly prior to mouse sacrifice (see table of materials; **Figure 4D**). Macrophages and T-cells can be visualized by using the anti-CD301-PhycoErythrin antibody (see table of materials; **Figure 4D**) and the anti-TCR- β -Pacific Bleu antibody (see table of materials; **Figure 4E**). The peripheral nerve network can be detected by using the anti-Tyrosine Hydroxylase (TH) antibody (see table of materials; **Figure 4F-G**). Additionally, this protocol allows the clearing of mouse epididymal adipose tissue (**Figure 4A-B, E**), mouse subcutaneous adipose tissue (**Figure 4D, G**), mouse brown adipose tissue (**Figure 4F**), and human adipose tissue (**Figure 4C**). Using a combination of these labelling and a commercial software (see table of materials) to segment these markers, we can determine within the adipose tissue i) adipocytes mean size and size distribution (**Figure 5A-B**) and ii) blood vessel network density (**Figure 5C**).

FIGURE LEGENDS:

Figure 1. Summary of the clearing procedure for white adipose tissue. Mouse or human white

adipose tissues are fixed, permeabilized, saturated, stained and cleared. Images are then acquired in 3D and analyzed using a commercial software.

Figure 2. Photographs of white adipose tissue. (A) Photograph of human white abdominopelvic adipose tissue before and after the clearing procedure. (B) Photograph of mouse epididymal white adipose tissue before and after the clearing procedure.

Figure 3. Improved imaging depth with adipose tissue clearing. (A) Mounting of the metallic imaging chamber equipped with glass bottom. (B) Z-series images of mouse epididymal white adipose tissue stained with phalloidin-Alexa488 (green) before and after clearing. (C) XZ projections corresponding to the white dotted lines across the panel B z-stack. (D) Z-projection of 0.4 cm z-stack of mouse subcutaneous white adipose tissue stained for actin using Phalloidin-Alexa488 and acquired at low magnification with a 4x objective. The small images on the right were acquired at the selected tissue position using a 20x objective. (E) Side view of the 3D volume rendering of image z-stack from cleared mouse white adipose tissue stained with Phalloidin-Alexa488 acquired similarly to the 20x images from (D). The 3D imaging depth achieved by our high magnification procedure is demonstrated here and underlined by a z-depth color coding (dark blue for z=0 mm to dark red for z=2 mm).

Figure 4. Mouse and human white adipose tissues stained for several markers. (A) Single plane image of mouse epididymal white adipose tissue stained for lipid droplets using anti-perilipin1 antibody and anti-mouse-alexa647-conjugated antibody. (B) Mosaic single plane image of mouse epididymal white adipose tissue stained for nuclei and adipocytes using DAPI, anti-Glut4 antibody and anti-mouse-alexa647-conjugated antibody. (C) Z-projection of 600 μ m z-stack of human white abdominopelvic adipose tissue stained for vessels using CD31-alexa647-conjugated antibody. (D) Z-projection of 600 μ m z-stack of mouse subcutaneous white adipose tissue stained for vessels and macrophages using lectin-DyLight649 intravenous injections and anti-CD301-alexa555 antibody. The lower right inset is a zoomed image of the white dotted box. (E) Single plane image of mouse epididymal white adipose tissue stained for actin and T-cells using phalloidin-Alexa488 and anti-TCR β -Pacific blue-conjugated. The lower right inset is a zoomed image of the white dotted box. (F) Z-projection of 50 μ m z-stack of mouse brown adipose tissue stained for nuclei and neuronal network using DAPI, anti-TH antibody and anti-rabbit-alexa647-conjugated antibody. (G) Z-projection of 600 μ m z-stack of mouse subcutaneous white adipose tissue stained for nuclei and neuronal network using DAPI, anti-TH antibody and anti-rabbit-alexa647-conjugated antibody.

Figure 5. Analysis of 3D images using commercially available software (see table of materials). (A) 3D volume rendering of human adipocytes segmented in 3D by commercially available software. Every adipocyte has a different color to its contacting adjacent adipocytes. Vessels are represented in red. (B) Size quantification and distribution of the adipocytes from the 3D volume rendering of panel A, which contains around 20,000 adipocytes. (C) 3D volume rendering of blood vessels segmented in 3D using commercially available software and represented in red or yellow for the large and small vessels, respectively.

Supplementary Movie 1. 3D volume rendering of the whole subcutaneous white adipose tissue shown in Figure 3D. The white box represents a 2 cm³ cube.

DISCUSSION:

The modifications that occur within the adipose tissue over the course of pathological progression, such as that of obesity, is fundamental to the understanding of the mechanisms behind the pathology. Pioneering studies that revealed such mechanisms in adipose tissue have been based on global approaches such as whole adipose tissue proteomics²¹, flow cytometry^{22,23}, and transcriptomics^{24,25}. In addition, efforts have been made to explore the structural changes occurring in adipose tissue using histological analyses²⁶⁻²⁹. However, the analysis of 5-10 µm adipose tissue sections, because of the limited size of the section, restricts the ability to appreciate important structural features. First, only a few adipocyte nuclei are detectable per section since each section represents only a small portion of the adipocytes (1/10th). Second, the size of the adipocytes estimated from adipose tissue sections is inaccurate because most adipocytes are cut below or behind their equator, leading to a biased (under)measurement of their mean size. Third, the blood vessel and nerve fiber continuum are lost during physical sectioning. Fourth, the distribution of each subtypes of immune cells within the tissue is difficult to establish because the three-dimensional coordinates are lost. In this context, the methodology we propose here allows any standard laboratory to image human and mouse white adipose tissue in three-dimensions, in a simple and inexpensive manner.

This method does have some limitations. First, the time required to prepare the tissue (fixation, permeabilization, staining, clearing) is long (more than a week). This would be difficult to reduce because the majority of this time is required to stain the tissue. The penetration of antibodies within such large tissue samples requires long incubation times. Decreasing the incubation time would increase the risk of having non-homogenous antibody penetration, which would lead to staining artifacts. Therefore, the only possible window to gain time and shorten the procedure is the time dedicated to clear the tissue, which takes around one day when optimal results are required, but this can be decreased to half a day without a dramatic drop in quality. The second limitation is the probable shrinkage of the tissue. Indeed, in any protocol that dehydrates tissue using solvents, it is likely that the tissues shrink due to water removal. Estimating this shrinkage is always challenging, and it is nearly impossible here because the edge of the tissue becomes transparent when lipids start to be extracted during the dehydration process. Hence, the size estimations of the cleared tissues need to be interpreted with caution. However, comparing changes in adipocyte sizes or vessel length between tissues derived from mouse with different genotypes and/or submitted to different environmental conditions remain informative¹¹. The last limitation is linked to the large volume of the whole mouse adipose tissue or of a large human adipose tissue surgical sample. Indeed, although the protocol is perfectly adapted to clear these large samples, imaging a whole organ is challenging with a confocal microscope. The strategy to overcome this issue and to exploit the full potential of the whole organ clearing procedure, is to acquire a 3D low magnification map of the whole organ by using a 4x objective, and to select specific areas randomly dispersed within the tissue where higher magnification 3D images using a 20x long-distance objective can be acquired. The “high magnification” setup allows imaging the tissue volume of around 45

mm³ (4.7 x 4.7 x 2 mm). Although this volume is limited compared to the volume of the whole organ (0.5 to more than 4cm³), repeating the acquisitions at several positions within the tissue allows us to obtain a good sampling of the tissue at cellular to sub-cellular resolution. Note that imaging large tissues will generate a significant amount of imaging data that will need to be stored.

The procedure has significant differences when compared to methods that have previously been described to clear adipose tissue^{14,30}. First of all, unlike AdipoClear, that uses methanol, dichloromethane, and dibenzylether¹⁴, the method presented here uses ethanol for dehydration and methyl salicylate for clearing. Therefore, the procedure is safer because it takes advantage of less toxic clearing solvents that are often used by food/drink-processing industries (ethanol and methylsalicylate), in comparison to the high toxicity of dichloromethane, methanol and dibenzylether. Moreover, the preparation of the tissue according to the protocol is two days faster than the AdipoClear protocol¹⁴. More recently, another method was proposed by Li and colleagues to clear adipose tissue pieces by immersing them into glycerol³⁰. This protocol is very simple even compared to this procedure, and the quality of the images is good even at high magnification. However, this clearing protocol only works efficiently when using 2 mm³ adipose tissue pieces. The sectioning of the tissue into these tiny samples prior to the clearing procedure prevents one from imaging tissue volumes larger than 2 mm³ even at low magnification. The procedure presented here allows mapping of the whole tissue in 3D at low magnification and acquisition of 3D stacks of images around 45 mm³ at several known positions within the whole cleared adipose tissue at high magnification.

This procedure may have several future applications. As with any method, the procedure described here can be simplified and/or further optimized. An interesting advance for the procedure could come from the combination of the clearing process, we described, with additional imaging approaches. For example, specific imaging setups, such as Optical Projection Tomography (OPT), Total Internal Reflection Fluorescence microscopy (TIRF), Selective Plane Illumination Microscopy (SPIM) or Stimulated Emission Depletion microscopy (STED) are in principle compatible with the procedure, although this will limit its applicability to those laboratories that are equipped with these systems. Alternatively, using an objective with a high numerical aperture index and an acquisition system that is able to acquire hundreds of images per second, which is found in many laboratories, one could perform super-resolution analyses by using the Super Resolution Radial Fluctuations (SRRF) post-processing image analysis freeware³¹. Interestingly, classical fluorochromes are adapted for the SRRF analysis, which would enable 3D super-resolution analyses of whole human and mouse white adipose tissues.

Many critical steps in the protocol are related to the tissue processing prior to the clearing itself. First of all, and as for classical histological analyses, the fixation step is fundamental. In the case of weak fixation, structural features are not preserved, whereas extended fixation leads to crosslinking and blocking of specific antigen sites and consequent non-homogeneous immuno-staining. Another sensitive step is the staining of the tissue, which presents several critical points that we will describe below. First, the antibodies need to be validated by testing them on cryostat sections to confirm that they are functional and to determine their optimal

concentration. The final concentration that is used for the clearing procedure is ten times the optimal concentration for the cryostat sections. Second, the time of incubation is also critical because of the size of the tissue. An incubation time that is too short will produce weak or non-homogeneous immunostaining (e.g., correct staining on the periphery of the tissue but no internal staining). Similarly, washing steps that are too short will prevent non-specifically-bound antibodies from being removed from the tissue leading to non-specific staining. To our knowledge, extended incubation of the tissue with antibodies does not impair the staining. Therefore, we strongly recommend long incubation and washing periods. Third, the choice of the fluorochrome must be adapted to the signal of interest. In tissue samples in general, and especially white adipose tissue, non-negligible auto-fluorescence is detectable at 488 nm and 555 nm. For highly expressed proteins this is not an issue and the staining will work well in these channels. However, for proteins with low expression we strongly recommend the use of far-red fluorochromes. For the clearing, there are no critical steps since the methodology is very simple. Keep in mind that methyl salicylate is not compatible with plastic materials, therefore we recommend glass bottles for the clearing steps and a metallic chamber equipped with a glass bottom to perform the imaging. Alternatives for this mounting procedure exist using i) a normal glass slide, dental resin and glass coverslip (to generate a small glass chamber), or ii) a glass petri-dish (for upright microscope setups).

ACKNOWLEDGMENTS:

This work was supported by INSERM, Université Côte d'Azur, and by grants from the French National Research Agency (ANR) through the Investments for the Future Labex SIGNALIFE (ANR-11-LABX-0028-01), the program UCA JEDI (ANR-15-IDEX-01) via Academy 2 "Systèmes Complexes" and Academy 4 "Complexité et diversité du vivant", and the Young Investigator Program to J.G. (ANR18-CE14-0035-01-GILLERON). We also thank the Imaging Core Facility of C3M funded by the Conseil Départemental des Alpes-Maritimes and the Région PACA, and which is also supported by the IBISA Microscopy and Imaging Platform Côte d'Azur (MICA). We thank Marion Dussot for technical help in tissue preparation. We thank Abby Cuttriss, UCA International Scientific Visibility, for proof reading of the manuscript.

DISCLOSURES:

The authors have no conflicts to disclose.

REFERENCES:

- 1 Pellegrinelli, V., Carobbio, S., Vidal-Puig, A. Adipose tissue plasticity: how fat depots respond differently to pathophysiological cues. *Diabetologia*. **59** (6), 1075-1088 (2016).
- 2 Stern, J. H., Rutkowski, J. M., Scherer, P. E. Adiponectin, Leptin, and Fatty Acids in the Maintenance of Metabolic Homeostasis through Adipose Tissue Crosstalk. *Cell Metabolism*. **23** (5), 770-784 (2016).
- 3 Mittendorfer, B. Origins of metabolic complications in obesity: adipose tissue and free fatty acid trafficking. *Current Opinion in Clinical Nutrition & Metabolic Care*. **14** (6), 535-541 (2011).
- 4 Hammarstedt, A., Gogg, S., Hedjazifar, S., Nerstedt, A., Smith, U. Impaired Adipogenesis and Dysfunctional Adipose Tissue in Human Hypertrophic Obesity. *Physiological Reviews*. **98** (4),

1911-1941 (2018).

5 Moreno-Indias, I., Tinahones, F. J. Impaired adipose tissue expandability and lipogenic capacities as ones of the main causes of metabolic disorders. *Journal of Diabetes Research*. **2015**, 970375 (2015).

6 Vergoni, B. et al. DNA Damage and the Activation of the p53 Pathway Mediate Alterations in Metabolic and Secretory Functions of Adipocytes. *Diabetes*. **65** (10), 3062-3074 (2016).

7 Xue, Y., Xu, X., Zhang, X. Q., Farokhzad, O. C., Langer, R. Preventing diet-induced obesity in mice by adipose tissue transformation and angiogenesis using targeted nanoparticles. *Proceedings of the National Academy of Sciences U S A*. **113** (20), 5552-5557 (2016).

8 Zwick, R. K. et al. Adipocyte hypertrophy and lipid dynamics underlie mammary gland remodeling after lactation. *Nature Communication*. **9** (1), 3592 (2018).

9 Zhang, L. et al. The inflammatory changes of adipose tissue in late pregnant mice. *Journal of Molecular Endocrinology*. **47** (2), 157-165 (2011).

10 Yang, H. et al. Obesity increases the production of proinflammatory mediators from adipose tissue T cells and compromises TCR repertoire diversity: implications for systemic inflammation and insulin resistance. *Journal of Immunology*. **185** (3), 1836-1845 (2010).

11 Laforest, S. et al. Comparative analysis of three human adipocyte size measurement methods and their relevance for cardiometabolic risk. *Obesity (Silver Spring)*. **25** (1), 122-131 (2017).

12 Azaripour, A. et al. A survey of clearing techniques for 3D imaging of tissues with special reference to connective tissue. *Progress in Histochemistry and Cytochemistry*. **51** (2), 9-23 (2016).

13 Richardson, D. S., Lichtman, J. W. Clarifying Tissue Clearing. *Cell*. **162** (2), 246-257 (2015).

14 Chi, J., Crane, A., Wu, Z., Cohen, P. Adipo-Clear: A Tissue Clearing Method for Three-Dimensional Imaging of Adipose Tissue. *Journal of Visualized Experiments*. 10.3791/58271 (137) (2018).

15 Roberts, D. G., Johnsonbaugh, H. B., Spence, R. D., MacKenzie-Graham, A. Optical Clearing of the Mouse Central Nervous System Using Passive CLARITY. *Journal of Visualized Experiments*. 10.3791/54025 (112) (2016).

16 Woo, J., Lee, M., Seo, J. M., Park, H. S., Cho, Y. E. Optimization of the optical transparency of rodent tissues by modified PACT-based passive clearing. *Experimental & Molecular Medicine*. **48** (12), e274 (2016).

17 Zhang, Y. et al. 3D imaging of optically cleared tissue using a simplified CLARITY method and on-chip microscopy. *Science Advances*. **3** (8), e1700553 (2017).

18 Ke, M. T., Imai, T. Optical clearing of fixed brain samples using SeeDB. *Current Protocols in Neuroscience*. **66**, Unit 2 22 (2014).

19 Hahn, C. et al. High-resolution imaging of fluorescent whole mouse brains using stabilised organic media (sDISCO). *Journal of Biophotonics*. **12** (8), e201800368 (2019).

20 Spalteholz, W. Über das Durchsichtigmachen von Menschlichen und Tierischen Präparaten und Seine Theoretischen Bedingungen. S. Hirzel, Leipzig. (1911).

21 Shields, K. J., Wu, C. Differential Adipose Tissue Proteomics. *Methods in Molecular Biology*. **1788**, 243-250 (2018).

22 Bourlier, V. et al. Remodeling phenotype of human subcutaneous adipose tissue

573 macrophages. *Circulation*. **117** (6), 806-815 (2008).

574 23 Hagberg, C. E. et al. Flow Cytometry of Mouse and Human Adipocytes for the Analysis of

575 Browning and Cellular Heterogeneity. *Cell Reports*. **24** (10), 2746-2756 e2745 (2018).

576 24 Hill, D. A. et al. Distinct macrophage populations direct inflammatory versus

577 physiological changes in adipose tissue. *Proceedings of the National Academy of Sciences U S A*.

578 **115** (22), E5096-E5105 (2018).

579 25 Acosta, J. R. et al. Single cell transcriptomics suggest that human adipocyte progenitor

580 cells constitute a homogeneous cell population. *Stem Cell Research & Therapy*. **8** (1), 250

581 (2017).

582 26 Coppack, S. W. Adipose tissue changes in obesity. *Biochemical Society Transactions*. **33**

583 (Pt 5), 1049-1052 (2005).

584 27 Cencello, R. et al. Reduction of macrophage infiltration and chemoattractant gene

585 expression changes in white adipose tissue of morbidly obese subjects after surgery-induced

586 weight loss. *Diabetes*. **54** (8), 2277-2286 (2005).

587 28 Cinti, S. Adipocyte differentiation and transdifferentiation: plasticity of the adipose

588 organ. *Journal of Endocrinology Investigation*. **25** (10), 823-835 (2002).

589 29 Wellen, K. E., Hotamisligil, G. S. Obesity-induced inflammatory changes in adipose

590 tissue. *Journal of Clinical Investigation*. **112** (12), 1785-1788 (2003).

591 30 Li, X., Mao, Z., Yang, L., Sun, K. Co-staining Blood Vessels and Nerve Fibers in Adipose

592 Tissue. *Journal of Visualized Experiments*. 10.3791/59266 (144) (2019).

593 31 Gustafsson, N. et al. Fast live-cell conventional fluorophore nanoscopy with ImageJ

594 through super-resolution radial fluctuations. *Nature Communication*. **7**, 12471 (2016).

595

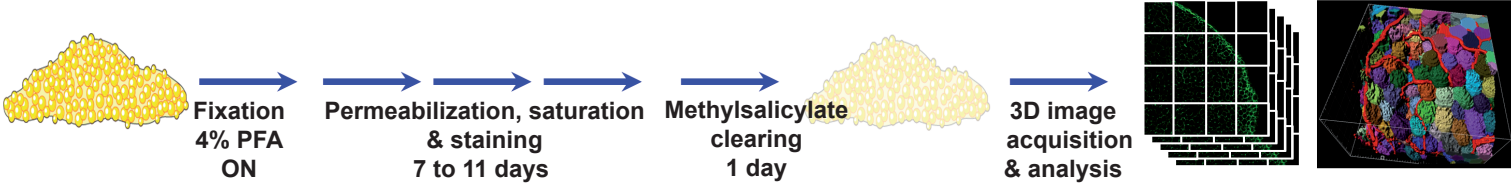


Figure 1

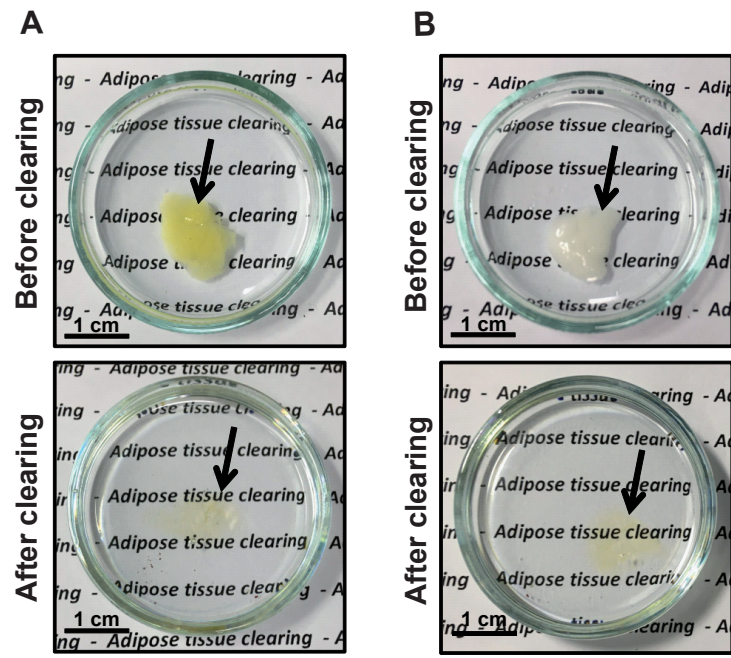
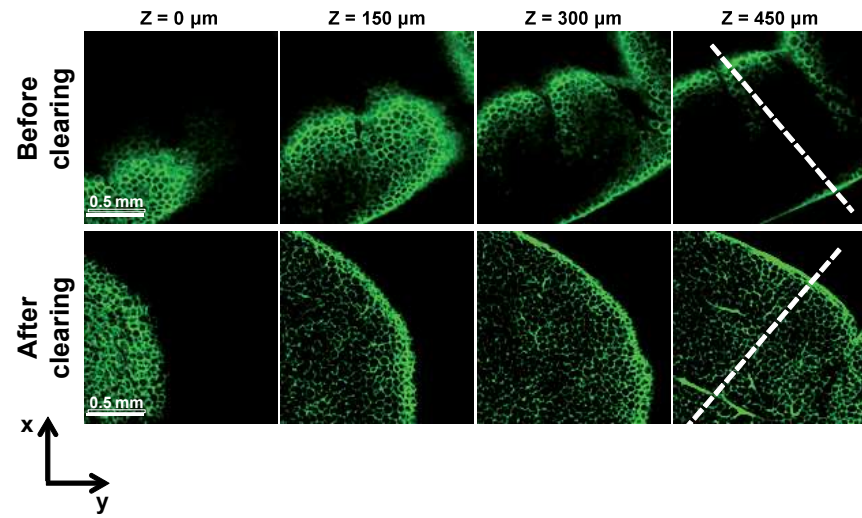
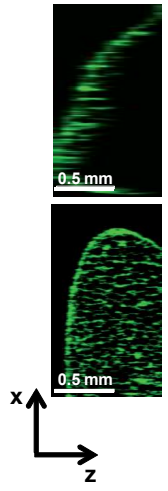
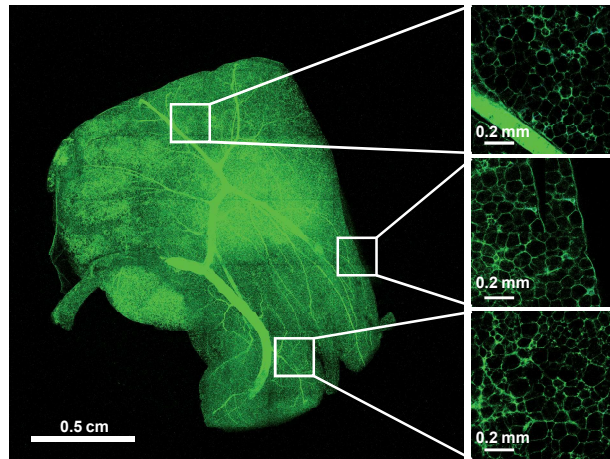
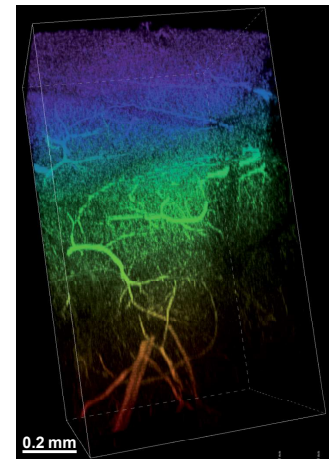


Figure 2

A**B****C****D****E****Figure 3**

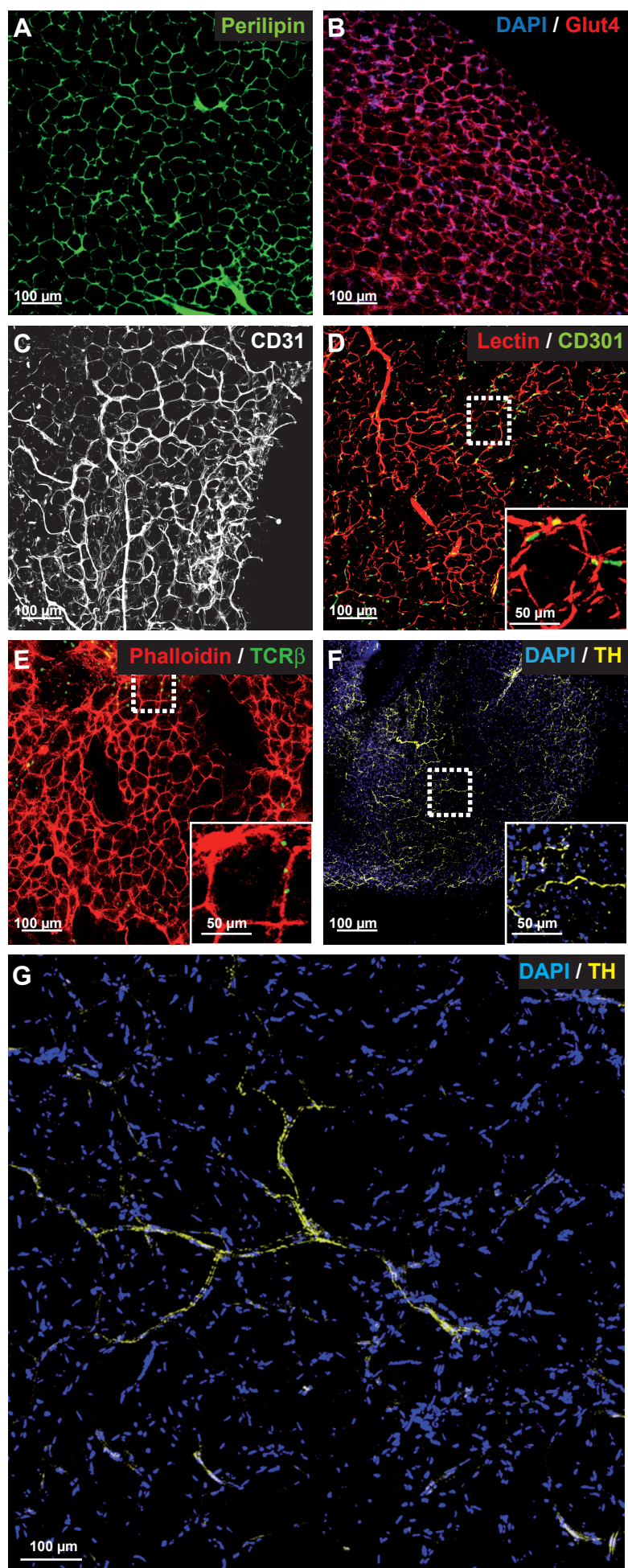


Figure 4

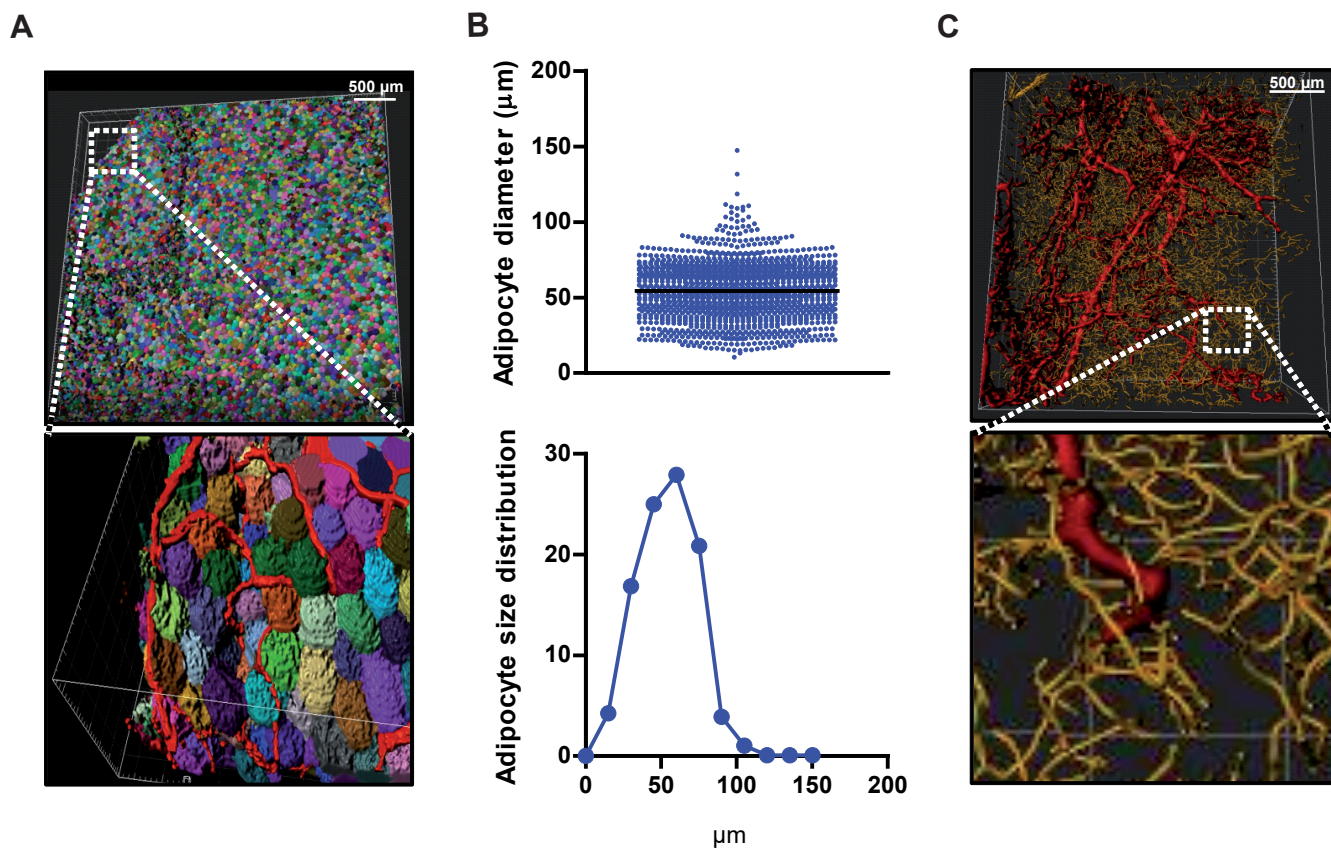
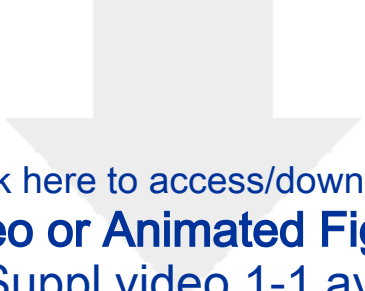
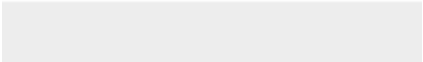



Figure 5



Click here to access/download
Video or Animated Figure
Suppl video 1-1.avi



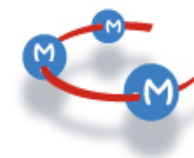
Name of Material/Equipment	Company	Catalog Number	Comments/Description
1.5 mL microtubes	Eppendorff tubes - Dutscher	33528	
15 mL plastic tubes	Falcon tubes - Dutscher	352096	
18 mm round glass coverslip	Mariendfeld	0117580	
20 mL glass bottle	Wheaton	986546	
anti-mouse-alexa647-conjugated antibody	Jackson ImmunoResearch	715-605-150	Dilution: 1/100
anti-rabbit-alexa647-conjugated antibody	Jackson ImmunoResearch	711-605-152	Dilution: 1/100
BSA	Sigma-aldrich	A6003	
CD301-PE antibody	Biolegend	BLE145703	Dilution: 1/100
CD31 antibody	AbCam	ab215912	Dilution: 1/50
Commercial 3D analysis software - IMARIS	Oxford instrument		with Cell module
Confocal microscope - Nikon A1R	Nikon		
Dapi	ThermoFisher	D1306	Stock Concentration: 5 mg/mL; dilution 1/1000
Deoxycholate	Sigma-aldrich	D6750	
DMSO	Sigma-aldrich	D8418	
Glut4 antibody	Santa Cruz	sc-53566	Dilution: 1/50
Glycine	Sigma-aldrich	G7126	
Lectin-DyLight649	Vector Lab	DL-1178-1	Stock Concentration : 2 µg/µL; IV Injection: 50 µL/mice
Metallic imaging chamber equipped with glass bottom - AttoFluor Chamber	Thermofisher	A7816	
Methyl salicylate	Sigma-aldrich	M6752	
Perilipin antibody	Progen	651156	Dilution: 1/50
Phalloidin-alexa488	ThermoFisher	A12379	Dilution: 1/100
TCR-β-PB antibody	Biolegend	BLE109225	Dilution: 1/100
TH antibody	AbCam	ab112	Dilution: 1/50
Triton X100	Sigma-aldrich	X100	

Tween-20

Sigma-aldrich

P416

**Centre de Recherche Méditerranéen
de Médecine Moléculaire**
U 1065
Dr Jérôme GILLERON
Team 7



July 07th, 2020

Editors – *JoVE*

Dear Dr DSouza,

We would like to thank you for your email dated on June 10th, 2020 informing us about the editorial and peer-reviewed comments for our manuscript.

We addressed all the reviewers' comments and performed the required editing. We included a point by point response, to address all the editor' and reviewers' concerns (see below).

We hope that our manuscript can now be considered for publication in *JoVE*.

Please contact me if any further information is required.

Sincerely yours,

Dr. Jérôme GILLERON



Response to editorial Comments:

• *Please take this opportunity to thoroughly proofread the manuscript to ensure that there are no spelling or grammatical errors.*

Extensive grammar and style editing was performed by a native English speaker.

• *Protocol Detail: Please note that your protocol will be used to generate the script for the video, and must contain everything that you would like shown in the video. Please ensure that all specific details (e.g. button clicks for software actions, numerical values for settings, etc) have been added to your protocol steps. There should be enough detail in each step to supplement the actions seen in the video so that viewers can easily replicate the protocol.*

This was corrected in the current version of our manuscript.

• *Protocol Numbering: Please adjust the numbering of your protocol section to follow JoVE's instructions for authors, 1. should be followed by 1.1. and then 1.1.1. if necessary and all steps should be lined up at the left margin with no indentations. There must also be a one-line space between each protocol step.*

We corrected the formatting accordingly.

• *Protocol Highlight: After you have made all of the recommended changes to your protocol (listed above), please re-evaluate the length of your protocol section. There is a 10-page limit for the protocol text, and a 3-page limit for filmable content. If your protocol is longer than 3 pages, please highlight ~2.5 pages or less of text (which includes headings and spaces) in yellow, to identify which steps should be visualized to tell the most cohesive story of your protocol steps.*

1) *The highlighting must include all relevant details that are required to perform the step. For example, if step 2.5 is highlighted for filming and the details of how to perform the step are given in steps 2.5.1 and 2.5.2, then the sub-steps where the details are provided must be included in the highlighting.*

2) *The highlighted steps should form a cohesive narrative, that is, there must be a logical flow from one highlighted step to the next.*

3) *Please highlight complete sentences (not parts of sentences). Include sub-headings and spaces when calculating the final highlighted length.*

4) *Notes cannot be filmed and should be excluded from highlighting.*

We have highlighted the text accordingly.

• *Discussion: JoVE articles are focused on the methods and the protocol, thus the discussion should be similarly focused. Please ensure that the discussion covers the following in detail and in paragraph form (3-6 paragraphs): 1) modifications and troubleshooting, 2) limitations of the technique, 3) significance with respect to existing methods, 4) future applications and 5) critical steps within the protocol.*

We re-formatted the discussion accordingly.

• *References: Please spell out journal names.*



We corrected the format accordingly.

• *Commercial Language: JoVE is unable to publish manuscripts containing commercial sounding language, including trademark or registered trademark symbols (TM/R) and the mention of company brand names before an instrument or reagent. Examples of commercial sounding language in your manuscript are Sigma-Aldrich, (#D6750, (#A6003, Sigma-Aldrich, Eppendorf, Falcon, #986546, Wheaton), AttoFluor chamber #A7816, ThermoFisher, IMARIS, etc. 1) Please use MS Word's find function (Ctrl+F), to locate and replace all commercial sounding language in your manuscript with generic names that are not company-specific. All commercial products should be sufficiently referenced in the table of materials/reagents. You may use the generic term followed by "(see table of materials)" to draw the readers' attention to specific commercial names.*

We removed all the commercial language from the main text. In the current manuscript, we only mention the company in the table of materials to allow readers to reproduce our work.

• *If your figures and tables are original and not published previously or you have already obtained figure permissions, please ignore this comment. If you are re-using figures from a previous publication, you must obtain explicit permission to re-use the figure from the previous publisher (this can be in the form of a letter from an editor or a link to the editorial policies that allows you to re-publish the figure). Please upload the text of the re-print permission (may be copied and pasted from an email/website) as a Word document to the Editorial Manager site in the "Supplemental files (as requested by JoVE)" section. Please also cite the figure appropriately in the figure legend, i.e. "This figure has been modified from [citation]."*

Not relevant, the figures are original and unpublished.



Response to reviewer comments:

Reviewer #1:

Manuscript Summary:

The protocol by Gilleron et al. provided a detailed method for staining and clearing whole white fat pads either from human or mice. Overall, the protocol is well described. Details in each steps, necessary notes, and representative figures are sufficiently provided. However, before this protocol is published in JoVE, several points are required to be addressed.

We would like to thank the reviewer for these positive comments concerning our manuscript, especially that he/she finds it to be “well described”, and for which “details in each steps, necessary notes, and representative figures are sufficiently provided”

Major Concerns:

1. The authors failed to cite and compare their protocol with a previously published protocol in JoVE (Li X, et al. 2019. doi: 10.3791/59266). In the protocol by Li et al., they have utilized a even simpler clearing step but achieved a high-quality staining and image acquisition of adipose tissue blood vessels and nerve fibers.

The reviewer is correct that we were not comparing our protocol with the protocol of Li and colleagues in the first version of our manuscript. We agree that the protocol of Li and colleagues is even simpler and produces reasonable resolution, but their protocol is optimized and therefore limited to very small samples (around 2mm³), as clearly stated in their manuscript. This volume corresponds to a cube of tissue with 1.3 mm sides. The volume of the whole adipose tissue of mice that are fed a normal diet is around 0.6 cm³ and in mice fed a high fat diet it is close to 4cm³. Therefore, the protocol developed by Li and colleagues is not optimal for the analysis of large adipose tissues. Here, using our procedure, we manage to clear a few cm³ of mouse and human adipose tissue. We can therefore acquire the whole tissue at low magnification (e.g. 4x objective), and select several areas where to acquire higher magnification (e.g. 20x objective) 3D stacks of images representing each a volume of at least 45mm³. Such an approach allows to obtain a sampling of the tissue. We corrected the manuscript by implemented this information in the discussion.

2. Is this protocol also applied to brown fat pads?

This protocol also works well for brown adipose tissue and other tissues including liver, kidney, lung and whole embryos. In line with the reviewer's question we decided to include a picture of cleared mouse brown adipose tissue stained for the Tyrosin Hydroxylase (TH, see new **Figure 4F**).

3. Have the authors stained with nerve fiber markers?

Yes, we successfully performed experiments with an anti-TH antibody. We have now included these data in the revised version of the manuscript (see new **Figure 4F-G**).



Reviewer #2:

The manuscript "Exploring adipose tissue structure by clearing 3D whole-organ imaging" describes an approach for straightforward imaging of adipose tissues in mice and humans. This builds on a variety of whole mount and tissue clearing approaches that have been used to image different organs, including adipose tissue.

The manuscript would benefit from attention to the following major and minor points:

Major points:

1. The manuscript requires extensive editing for grammar and style.

We asked a native English speaker to perform extensive grammar and style editing.

2. Although the authors claim this method to be whole organ clearing and imaging, based on the described steps, this method does not have the capacity to do so. The authors should instead describe the method as "whole mount" clearing and imaging.

a. In Note 1, the authors specifically stated that they usually cut tissues into small pieces for this procedure. The staining and imaging steps in the main protocol (i.e. buffer volumes, incubation time, and antibody dilutions) are designed for handling small tissue chunks instead of whole tissue.

b. In step 5.3., the authors mentioned the z-stacks typically obtained by confocal microscopes are between 600 to 2000 micrometers. Since the authors suggested applying this method to study hypertrophy and hyperplasia in obese adipose tissue, obese fat pads easily surpass the 2 mm limit, and therefore cannot be imaged as a "whole organ" by the described method.

The method described herein successfully cleared the whole adipose tissue from mice fed either a normal or a high fat diet. There is no need to cut it into small tissue chunks for the clearing procedure.

a- We disagree with the comments of the reviewer suggesting that our procedure is designed for handling small tissue chunks instead of the whole tissue. First, a tissue with a volume of $1\text{g} - 2.5\text{cm}^3$ is 4 times bigger than the volume of an adipose tissue from mice fed a normal diet ($250\text{mg} - 0.6\text{cm}^3$), and represent more than 2/3 of the maximal volumes that can reach a whole adipose tissue from mice fed a high fat diet ($1.5\text{g} - 4\text{cm}^3$). Second, as clearly stated in our procedure, the clearing of the whole adipose tissue from mice fed a high fat diet can be easily done by linearly adapting the volume of the different buffers to the increase in adipose tissue mass. We designed the protocol to a volume of 1g because we find it sufficient to correctly appreciate the morphological changes occurring within the tissue.

b- We understand the concern of the reviewer concerning the step 5.3. This is because we were not clear enough about the imaging strategy we applied to take advantages of our ability to clear a whole organ, but taking also into account the depth limit range of around 3mm of the 20x long-distance objective we used to obtain high magnification images. Indeed, the whole organ can be imaged in 3D at low magnification (e.g. 4x objective) to appreciate its global structure (see the left image in Figure 3D). This large 3D stack can serve as a map to select several areas for imaging the tissue at higher magnification (e.g. 20x objective) spread within the tissue. We acknowledge that using the higher magnification set up to obtain images at sub-cellular resolution; we are able to obtain 3D stacks of images representing each a volume of at least 45mm^3 . This is far from the whole tissue, but repeating the "high magnification" acquisition at several position within the tissue could allow to obtain a correct representative sampling of the tissue (see the right images of the Figure 3D).



We corrected the title and the text to put into perspective our claim about “whole organ clearing”. We also clarified the step 5.3 by adding novel informations about our imaging strategy.

3. The authors claimed one advantage of this method over the iDISCO-based clearing protocols is its efficiency. In Figure 1, the time required for the entire protocol adds up to 8-15 days, which is not actually significantly different from the iDISCO-based methods (10-14 days).

We believe that our procedure has several advantages compared to the previously described iDisco-based protocol. The gain of time remains only one of these advantages. We agree with the reviewer that this gain is minimal (a few days). This is due to the fact that the major part of the time is used to stain the tissue, and this time is unchangeable to avoid staining artifacts. Therefore, we corrected the discussion on the differences between our procedure and the iDISCO-based method accordingly.

Moreover, we also thank the reviewer for noticing that a mistake was present in the time-line of the Figure 1 (read 7 to 11 days rather than 7 to 14 days).

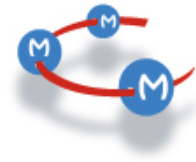
4. The sample images provided in the representative results section are not compelling.

a. Figure 3B: Even after clearing, phalloidin staining showed brighter signal towards the periphery but dimmer signal towards the center of the tissue, creating a halo effect. This is usually due to problems with antibody penetrance. The authors should address this issue as a limitation.

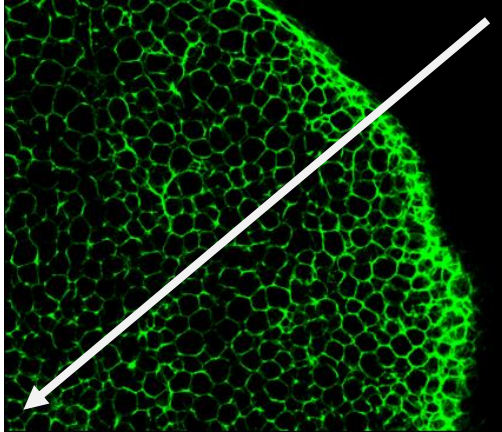
b. Figure 5A: The fat cells segmented by Imaris appear oval along the z-axis instead of spherical. The authors should address whether this is an actual reflection of the adipocyte shape or distorted during processing and imaging.

a/ We agree with the reviewer that the phalloidin staining is brighter at the very edge of the adipose tissue (one layer of cells) compared to the rest of the tissue. We do not believe that this is due to a problem of antibody penetration within the tissue, because such an issue would be visible in the form of a full gradient from the periphery toward the center of the tissue, which is not the case here. To demonstrate this, we plotted the intensity of phalloidin from the periphery of the tissue toward its center using the image presented in Figure 3B. As described below, except for the one-cell layer at the periphery, which is highly labeled with phalloidin, the rest of the signal is homogeneous and very similar high and low peaks are found both close to the center or at the periphery (see plot below). Similar results were found when using CD301 staining (from Figure 4D) – see below (the intensity of this marker is similar when macrophages are close to the center of the tissue or at the periphery). Moreover, the Glut4 staining (Figure 4B) does not present this high intensity at the periphery of the tissue. Altogether, these results suggest that antibody penetration is not responsible for the observation that phalloidin labeling is brighter at the periphery of the tissue. This high intensity in the outer layer of adipose tissue cells could be due to a specific high expression of actin in these non-adipocyte cells. Consistently, the peripheral cell layer of human and mouse adipose tissue lobules are known to be composed by a layer of mesothelial cells^{1,2}, which highly express actin relative to adipocytes. However, we agree with the reviewer that antibodies penetration problems could occur under specific conditions and ways to avoid it should be discussed. Therefore, we corrected the discussion accordingly.

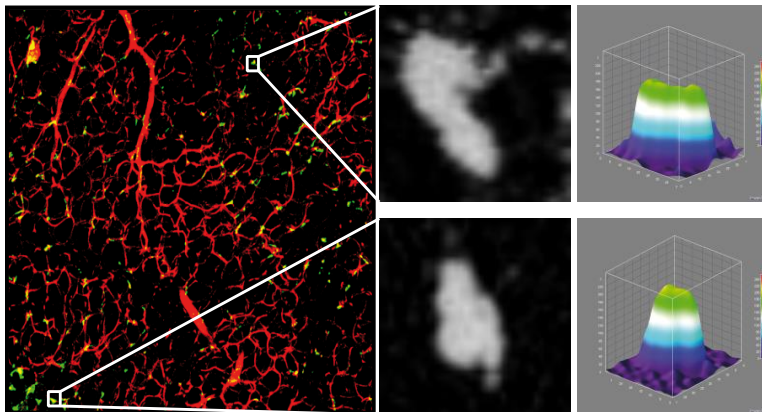
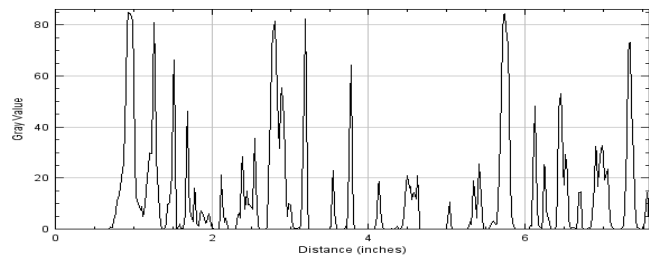
References:



1. Ivanov, S. et al. Mesothelial cell CSF1 sustains peritoneal macrophage proliferation. Eur J Immunol. 49 (11), 2012-2018, (2019).
2. Esteve, D. et al. Lobular architecture of human adipose tissue defines the niche and fate of progenitor cells. Nat Commun. 10 (1), 2549, (2019).

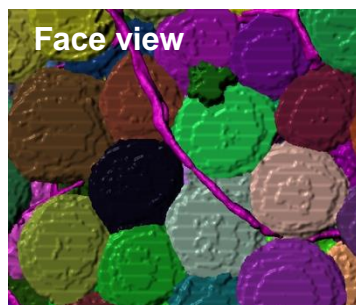


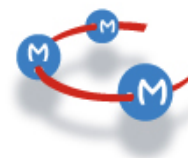
Phalloidin intensity along the white arrow



Intensity of CD301 signals in macrophages at the periphery and in the center of the adipose tissue.

b/ We think that this is just a false impression from the 3D view. Indeed, when we created a planar section from the xy direction or from the xz direction, we found mostly round adipocytes (see images below).





Minor points:

1. What is the advantage of using a high concentration of an antibody (10X) in a small volume of buffer? Why not use the same amount of antibody in a larger volume of buffer (1X)?

This is an interesting suggestion; we have never tested this possibility. Therefore, we are unable to predict whether having a similar amount of antibodies into a larger volume will improve, decrease or not modify the quality of the staining.

2. The authors should state which adipose depots were imaged in each figure.

We agree with the reviewer that this information is missing. We have added it to the revised version of the manuscript.

3. Tissue clearing was done with an ethanol gradient, which may cause shrinkage of tissue. Was there any shrinkage observed?

The problem of shrinkage highlighted by the reviewer is valide for all of the clearing protocols using solvents, and most likely independently of the solvents used (e.g. EtOH, methanol, DCM/DBE, etc.). Shrinkage is always difficult to estimate because one needs to compare it with native tissue, which in the case of adipose tissue is hard to image in depth without removing the lipids. Moreover, another difficulty comes from the fact that ethanol dehydration also removes lipids, starting to clear the peripheral parts of the tissues. This limits our capacity to correctly estimate the shrinkage of the tissue, although we believe that such shrinkage occurs. The reviewer correctly points out this limitation and we now discuss this in the revised version of the manuscript.

4. In Note 6, the authors described using several coverslips to prevent the tissue from floating in the chamber. Does this also prevent the tissue from moving around (sideways) during imaging?

The reviewer is correct. The coverslips also prevent tissue drift during imaging. We corrected the text accordingly.

5. The authors should provide more specifics on shaking. What speed was this done at?

We have corrected the text accordingly.

Reviewer #3:

Manuscript Summary:

This manuscript describes a relatively simple procedure for clearing white adipose tissues from mouse or human as well as suggestions for imaging via confocal microscopy and subsequent analysis in Imaris software. Unlike several recent methods that use methanol, dichloromethane, and dibenzyl ether, this method uses ethanol for dehydration and methyl salicylate for clearing.

We would like to thank the reviewer for noticing that our method is using different compounds for the clearing than the other methods previously described.

Major Concerns:

The table of required materials does not include any of the stains, dyes, or antibodies described in the "Representative Results" section. Ideally, these should be included as well as the concentrations/dilutions/incubation times used to generate the provided image data in the manuscript.

We agree with the reviewer and have completed the table accordingly.

Minor Concerns:



If possible, describe the sample sizes within the protocol as length measures (or cubic volume) instead of weight as some researchers may not be able to visualize what 1 gram of WAT looks like (at least provide it in addition to weight).

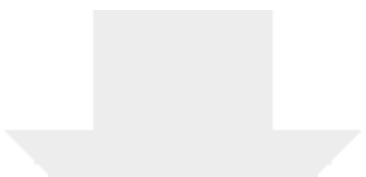
We agree with the reviewer that this information was missing. We estimated the cubic volumes of the tissues we usually analyze and provided this information.

- 1 Ivanov, S. *et al.* Mesothelial cell CSF1 sustains peritoneal macrophage proliferation. *Eur J Immunol.* **49** (11), 2012-2018, (2019).
- 2 Esteve, D. *et al.* Lobular architecture of human adipose tissue defines the niche and fate of progenitor cells. *Nat Commun.* **10** (1), 2549, (2019).

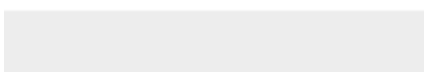
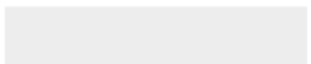


Click here to access/download
Supplemental Coding Files
Figure 1 JOVE gilleron.ai





Click here to access/download
Supplemental Coding Files
Figure 2 JOVE gilleron.ai









Click here to access/download
Supplemental Coding Files
Figure 5 JOVE gilleron.ai

